Behavior and Fate of Halloysite Nanotubes (HNTs) When Incinerating PA6/HNTs Nanocomposite

Ghania Ounoughene, Olivier Le Bihan, C. Chivas-Joly, C. Motzkus, C. Longuet, Bruno Debray, Aurélie Joubert, Laurence Le Coq, José-Marie Lopez-Cuesta

Environmental science and technology

Behavior and Fate of Halloysite Nanotubes (HNTs) When Incinerating PA6/HNTs Nanocomposite

G. Ounoughene,[†,‡,§] O. Le Bihan,[*,∥] C. Chivas-Joly,[⊥] C. Motzkus,[⊥] C. Longuet,[‡] B. Debray,[∥] A. Joubert,[†] L. Le Coq,[†] and J-M. Lopez-Cuesta[*,‡]

[†]LUNAM, Ecole des Mines de Nantes, GEPEA, CNRS, UMR 6144, 4 rue Alfred Kastler, 44307 Nantes Cedex 03, France

[‡]C2MA, Ecole des Mines d'Alès, 6 Avenue de Clavières, 30319 Alès Cedex, France

[§]ADEME, 20 avenue du Grésillé, 49004 Angers Cedex 01, France

[∥]INERIS, Parc Technologique Alata, 60550 Verneuil-en-Halatte, France

[⊥]LNE, 29 Avenue Roger Hennequin, 78197 Trappes Cedex, France

ABSTRACT: Nanoclay-based nanocomposites have been widely studied and produced since the late 1990s, and frequently end up in waste disposal plants. This work investigates the behavior of PA6/HNTs nanocomposites (nylon-6 incorporating halloysite nanotubes) during incineration. Incineration tests were performed at lab-scale using a specific tubular furnace modified in order to control the key incineration parameters within both the combustion and postcombustion zones. The combustion residues and combustion aerosol (particulate matter and gas phase) collected downstream of the incinerator furnace were characterized using various aerosol analysis techniques. Time tracking of the gas and particle-number concentrations revealed two-step char formation during combustion. HNTs transformed into other mineral structures which were found in both the aerosol and the residues. During combustion of the polymer, it appears that HNTs contribute to the formation of a cohesive char layer that protects the residual material.

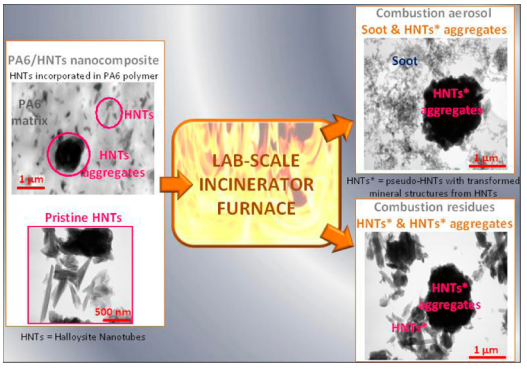

2. INTRODUCTION

In recent decades, polymer nanocomposites have drawn much attention due to their enhanced performance.[1−4] The physicochemical properties of polymer matrices (tensile strength, stiffness, heat resistance, barrier properties, etc.) are enhanced by adding small amounts of nano-objects. This is the case with polyamide 6 (PA6) incorporating silicate nanoclays. These nanocomposites have been extensively studied and developed by both universities and industry for many applications in various industrial areas such as transportation, electronic and electrical equipment, and packaging. Nevertheless, many of these state-of-the-art materials are expected to end up in waste treatment facilities such as incineration plants due to the lack of specific recovery procedures.[5] Hence, the potential environmental risk arising from the incineration of waste containing nanomaterials is a new field which deserves further attention. Some recent studies have begun to focus on this topic, but the data are incomplete.[5−12] The present study therefore gives some insight into the fate and behavior of nano-objects (incorporated in a polymer matrix) during the incineration of nanocomposites. The work focuses on PA6/HNTs nanocomposites (nylon-6 incorporating halloysite nanotubes).

Polyamide 6 (also called Nylon-6) is a semicrystalline polyamide thermoplastic used in a wide range of fiber, film and engineering applications. It has been shown that a small amount (1−10 wt %) of silicate nanofiller can remarkably enhance the properties of the material.[2,13] Nanofillers based on montmorillonite layered silicates have been the subject of many studies. More recently, halloysite nanotubes (HNTs) have also been studied, and have been reported to improve many properties, especially thermal properties, when incorporated in a PA6 polymer matrix.[14−17] HNTs are alumino-silicates. Their chemical composition is $Al_2Si_2O_5(OH)_4{,}2H_2O$. They are extracted from natural deposits and are chemically similar to kaolinite. Their nanotubular structure gives them very interesting properties that attract the attention of researchers for many applications.[17−19]

Many articles and book chapters have been published about the thermal degradation of nanocomposites,[13,16,20−25] but none of them relate to tests involving the combustion parameters of incineration (temperature around 850 °C, highly ventilated combustion, at least 2 s residence time for the combustion gas in a postcombustion chamber at 850 °C, and high oxygen/fuel contact) or time tracking of the gas and particle concentrations in the combustion aerosol. In the present work, we used a

laboratory scale furnace modified to control the key incineration parameters. The combustion aerosol was sampled downstream of the postcombustion chamber (i.e., analogous to upstream of filtration in a real-scale incineration plant), and was characterized using various aerosol analysis techniques. This was a first step in the evaluation of the efficiency of flue-gas cleaning systems. After that, the combustion residues were analyzed. The aim of this work is to study the behavior and the fate of HNTs during incineration of PA6/HNTs nanocomposites while investigating the influence of HNTs on combustion mechanisms (aerosol release and decomposition) and the release of nano-objects during incineration. It is relevant to ask whether the nano-objects initially incorporated in the polymer are destroyed or undergo changes during their stay in the incinerator and their fate thereafter.

3. MATERIALS AND METHODS

3.1. Sample Preparation and Characterization. PA6/HNTs nanocomposites (see Supporting Information (SI), Table S1) were prepared by melt extrusion and injection molding. The halloysite (shown in Figure 1) was provided by Imerys Ceramics from New Zealand. PA6 (polyamide 6) Technyl C206 was supplied by Rhodia Plastics Engineering SA. Neat matrix and two nanocomposites at two loadings (1 and 5%wt) of HNTs were prepared using the same extrusion and injection process to ensure the same thermo-chemical history for all samples. A twin-screw extruder (Clextral BC21, 1200 mm length) was used (rotational speed of 250 rpm, and processing temperature of 260 °C). The pelletized extruded material obtained was finally injection molded (Krauss Maffei KM50/180CX) into standard specimens ($100 \times 100 \times 4$ mm^3). 250 mg samples from these specimens were cut and then tested in the incinerator furnace.

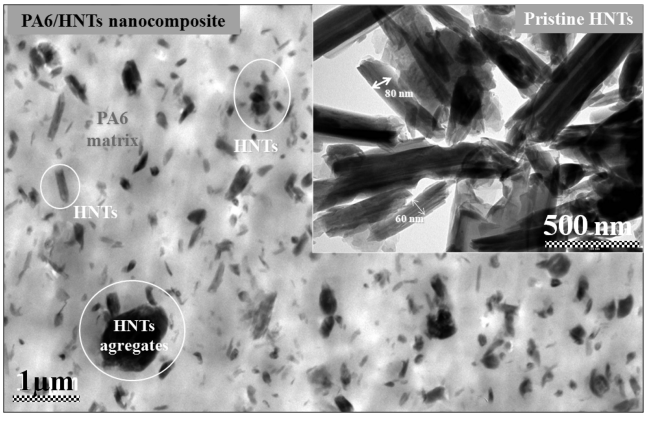

Figure 1. Pristine HNTs dispersed in PA6/HNTs nanocomposite.

The pristine HNTs and the prepared nanocomposite samples were characterized prior to the incineration tests. Imagery on pristine HNTs and on the dispersion of HNTs in the nanocomposite (Figure 1) was carried out using transmission electronic microscope (Philips CM12 TEM 200 kV). In addition, elemental analysis of the polymer material, laser diffraction and X-ray fluorescence analysis of pristine Halloysite were performed (see SI, Tables S2 and S3 and Figure S2). TEM micrographs show the nanotubular structure of the pristine halloysite (Figure 1). In agreement with literature,[14−18] the observed halloysite tubes are nanosized with a thickness lower than 100 nm.

Thermogravimetric analysis (TGA) was performed using a Pyris-1 Perkin−Elmer apparatus. Samples of 10 (±2) mg were heated under a nitrogen flow at a 10 °C/min heating rate from ambient temperature to 850 °C.

PCFC (pyrolysis combustion flow calorimeter) tests were carried out using a fire testing technology apparatus (FTT, ASTM D7309). A sample of 2 (±1) mg was heated under nitrogen flow to 750 °C at a heating rate equal to 1 K/s. Gases were extracted and sent to a combustion chamber in the presence of a N_2/O_2 flow (80/20). The combustor ensured complete oxidation of pyrolysis products at a combustion temperature fixed at 900 °C.[26]

3.2. Lab-Scale Incinerator and Analysis. Laboratory scale incineration tests were performed using a specific tubular furnace. The combustion conditions implemented in the lab-scale incinerator furnace (within both the combustion and postcombustion zones) were controlled to satisfy the key operational parameters that govern an incineration process, that is, chiefly temperature (850 °C in the combustion and postcombustion-zone), residence time (at least two seconds in the postcombustion zone at 850 °C), air-excess (never below 11% of oxygen) and turbulence (a good mix between combustible and oxygen). A tubular horizontal furnace (Carbolite STF 15/610 Horizontal Tube Furnace) was modified to obtain as close as possible to the combustion conditions implemented in an industrial grate incinerator. As illustrated in

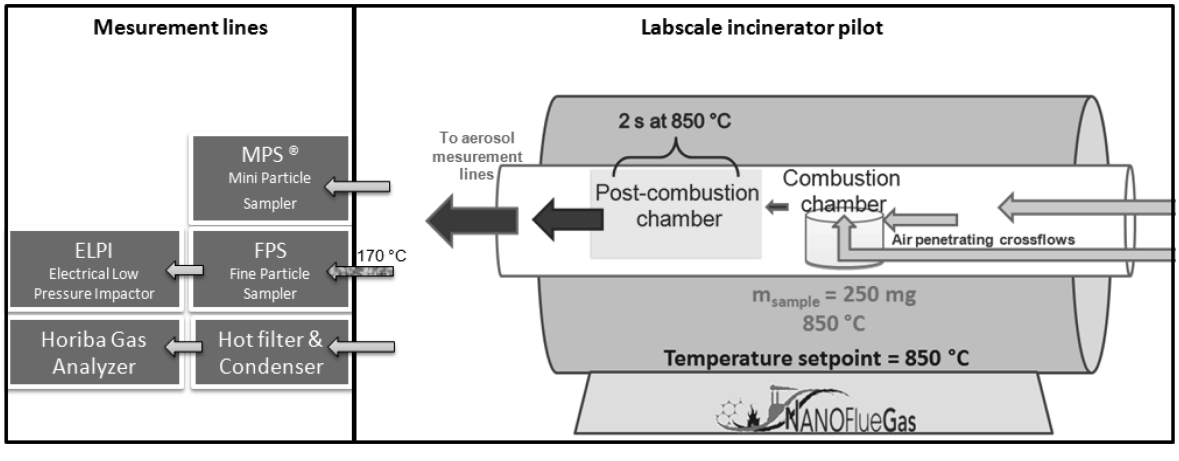

Figure 2. Basic diagram of the modified tubular furnace—Lab-scale incinerator and the measurement lines.

Figure 2 the "combustion chamber" is maintained at 850 °C (at least) and where air cross flows penetrate and mix with the combustibles. Then, the "post-combustion chamber" is the furnace zone where the combustion aerosol stays 2 s at 850 °C (at least).

Finally the combustion released gases and the aerosol particles were conveyed to the measurement line as described in the following paragraph.

In order to superimpose the curves of time tracking, it is important to know the response time of each measurement line to synchronize all events detected. The reaction time of each unit of the measurement line is determined by stopwatch. An uncertainty of two seconds is taken into account.

The combustion aerosol was sampled appropriately as explained below and analyzed in three different ways: time tracking for the gas and particles from the aerosol and two off-line analyses for the particulate matter. Further analyses were conducted on the combustion residues.

3.2.1. Time Tracking for the Gas Phase. The sampling of the gas phase from the combustion aerosol followed the methods used for sampling direct emissions from stationary combustion sources. The flue gas leaving the furnace was dried and filtered using a line with a hot filter and a condenser. A multigas analyzer (portable gas analyzer PG-250 Horiba) was used. It indicates the evolution of the combustion gases concentrations: the consumption of O_2 ($\%_{vol.}$) and the production of NOx ($ppm_{vol.}$), CO_2 ($\%_{vol.}$) and CO ($ppm_{vol.}$). They are respectively detected by paramagnetism, chemiluminescence and an infrared technique with 1 s time resolution.

3.2.2. Time Tracking and off-Line Analysis for Particulate Matter. The combustion aerosol sampled downstream of the postcombustion chamber has to be representative of the aerosol sampled upstream of the flue-gas cleaning systems. The target temperature is 170 (±10) °C. In fact, under industrial conditions, the aerosol leaves the postcombustion chamber and goes through an upstream filtration processes at a temperature around 150 °C in accordance with BREF Waste Incineration (2006).[27] Different samplers and impactors were used to conduct the analyses with respect to the temperature constraint mentioned above.

Regarding the time tracking of the particles from the combustion aerosol, an electrical low pressure impactor, Dekati (ELPI) was used downstream of a fine particle sampler dilutor (FPS, Dekati). The objective of the sampling was to avoid cold spots below 170 °C before and during the first dilution. FPS dilutor is well adapted to measurements related to combustion research. This system allows sampling from hot flue gas and provides controlled temperature decrease with minimal losses.[28−30] The FPS dilutor performs two successive dilutions: the first heated dilution at 170 °C and the second at room temperature. The primary dilution air was heated to 170 (±10) °C. Thus, the sampled combustion aerosol underwent two dilutions with a total factor of 1:30. The dilution ratio was given in real time by the FPS software. However, in order to check the displayed FPS value, the dilution ratio was recalculated continuously during the test using a gas analyzer connected to the output the FPS which indicates the concentration of CO and CO_2 after the dilution.[31]

The ELPI provided a real-time measurement of particle number concentration through 12 channels from 17 nm to 5 μm.[32] The $PN_{x\text{-}y}$ are defined as the number concentration of particles counted by the ELPI with mean geometric diameter (Di) between x and y μm.

Regarding off-line analyses, there were two types of sampling: in the first type, combustion aerosol particles were collected throughout the test; in the second type, combustion aerosol particles were collected over a targeted time range.

In the first case, the aerosol combustion underwent just one hot dilution at 170 °C with a porous tube dilutor from VTT laboratory (Valtion Teknillinen Tutkimuskeskus Technical research center of Finland).[33] This diluted hot sample was routed to a gravimetric impactor (DGI, Dekati Gravimetric Impactor) which was heated to the same temperature (170 °C ± 10 °C). This $PM_{2.5}$ four-stage impactor resolves particles into four size fractions with 50% collection efficiency for aerodynamic (dp50) cut-points of 2.5, 1.0, 0.5, 0.2 μm plus a back-up filter (after the impaction stages) which collects all particles typically smaller than 0.2 μm.[34] In this way, the particulate matter of the combustion aerosol was collected on PTFE impaction substrates with controlled temperature during sampling. Then, these particles were analyzed by a scanning electronic microscope (JEOL 7600F High Resolution Analytical SEM energy dispersive spectrometer SDD BRUKER (EDS) X-ray detector). This gravimetric impactor provided a qualitative analysis (imagery and chemistry) of particles collected during the whole combustion test.

In the second case, particles from the combustion aerosol were collected on a TEM grid for above 10 s downstream of the tubular furnace with a MPS (Mini-Particle-Sampler, Ecomesure[35]). A Philips CM12 TEM 200 kV was used for the imagery.

3.2.3. Analysis of the Combustion Residues. The combustion residues in the sample holder of the lab-scale incinerator were collected after each test. They were analyzed by TEM (Philips CM12 TEM 200 kV), and SEM. X-ray diffraction (XRD) with a Bruker AXS D8 Advance diffractometer using Cu Kα radiation.

4. RESULTS

4.1. Time Tracking of Gas Concentration and Particle Number Concentration. The graphs showing the evolution of concentrations during the incineration of the nanocomposite PA6/5HNTs are given in Figure 3a. The two verticals delimit the time range with more than 5% O_2 consumption from the baseline. This area of interest is denoted "AOI". The averages of three runs are presented with the associated standard deviation. When the neat matrix is compared to the nanocomposite, weight standardization was performed in order to compare the same mass of polymer.

Before the AOI, from 0 to 48 s, O_2 consumption is low, little gases are produced, but particles are strongly emitted with a domination of $PN_{0.1}$. Ignition is observed during this period. During the AOI, which extends over a period from 48 to 100 s, oxygen consumption is maximal. From 48 to 80 s, peaks of CO_2, CO and NOx are noticed while $PN_{x\text{-}y}$ decreases. From 80 to 100 s, a second peak of CO begins along with an increase in $PN_{0.1}$. After the AOI, from 100 s to the end (250 s) a shoulder in NOx concentration appears with a second peak of CO, particles are less and less emitted, and O_2 reaches its baseline.

High concentration levels are noticed here. Then, considering such high concentrations, coagulation/agglomeration phenomena must occur in the furnace. Even if the pilot does respect a residence time of two seconds, it would be difficult to say if these phenomena occur in a real scale industrial furnace. This is rightly a limit of an incinerator lab-scale pilot.

Figure 3b−d show the comparisons between neat PA6 and PA6/5HNTs nanocomposite. A second phase of particle

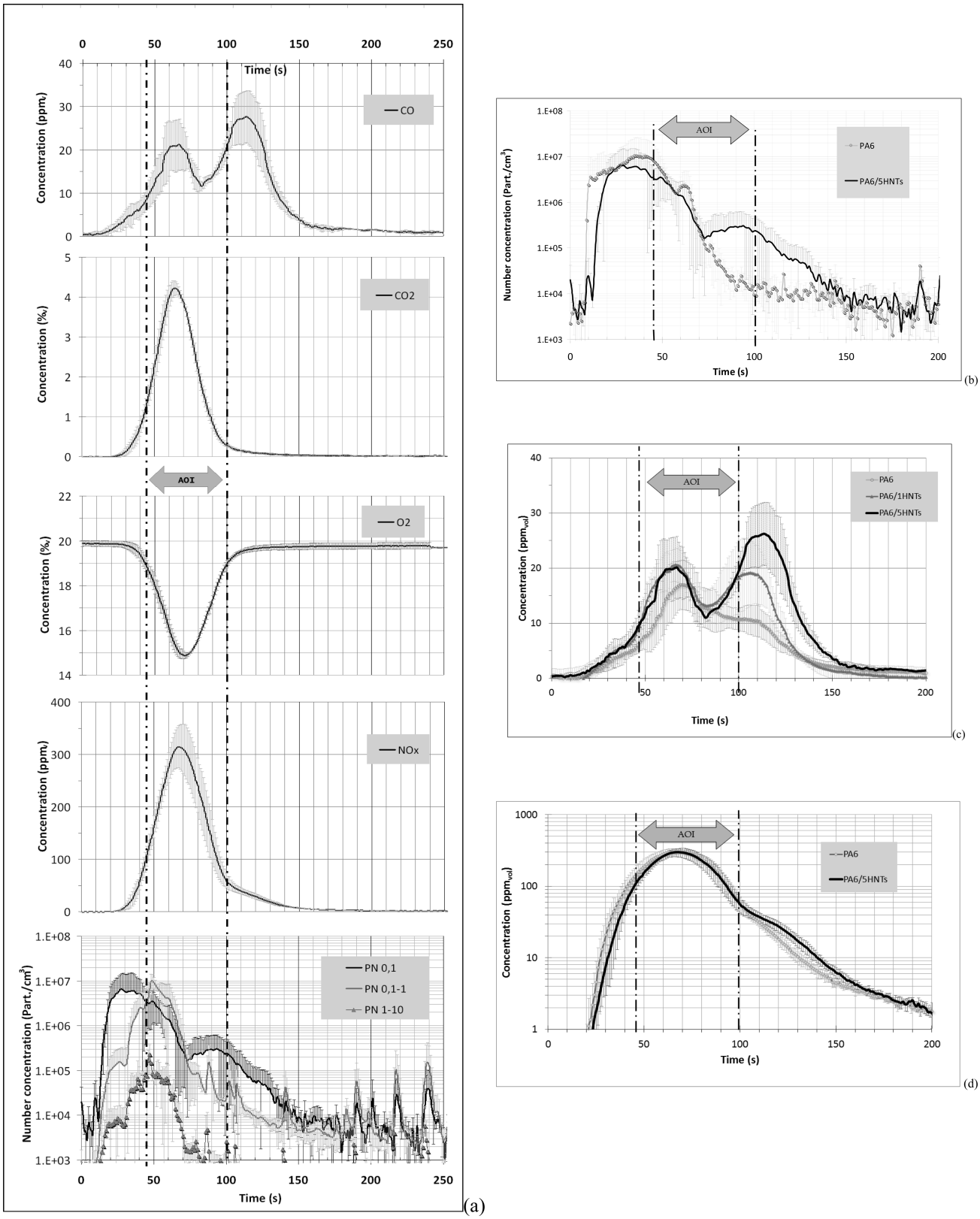

Figure 3. (a) Time tracking for PA6/5HNTs incineration: particle number concentration and gas concentration, (b) Comparison between PA6 and PA6/5HNTs for $PN_{0.1}$ concentration, (c) Comparison between PA6, PA6/5HNTs and PA6/1HNTs for CO concentration, (d) Comparison between PA6 and PA6/5HNTs for NOx concentration (log scale).

emission is clearly observed, as well as a shoulder in NO_x concentration and a second peak of CO but only for nanocomposite. This tendency is the same for PA6/1HNTs (Figure 3c) with its CO curve just inserted between the two other CO curves. Other time tracking comparisons show no significant differences (see SI, Figures S3 and S4).

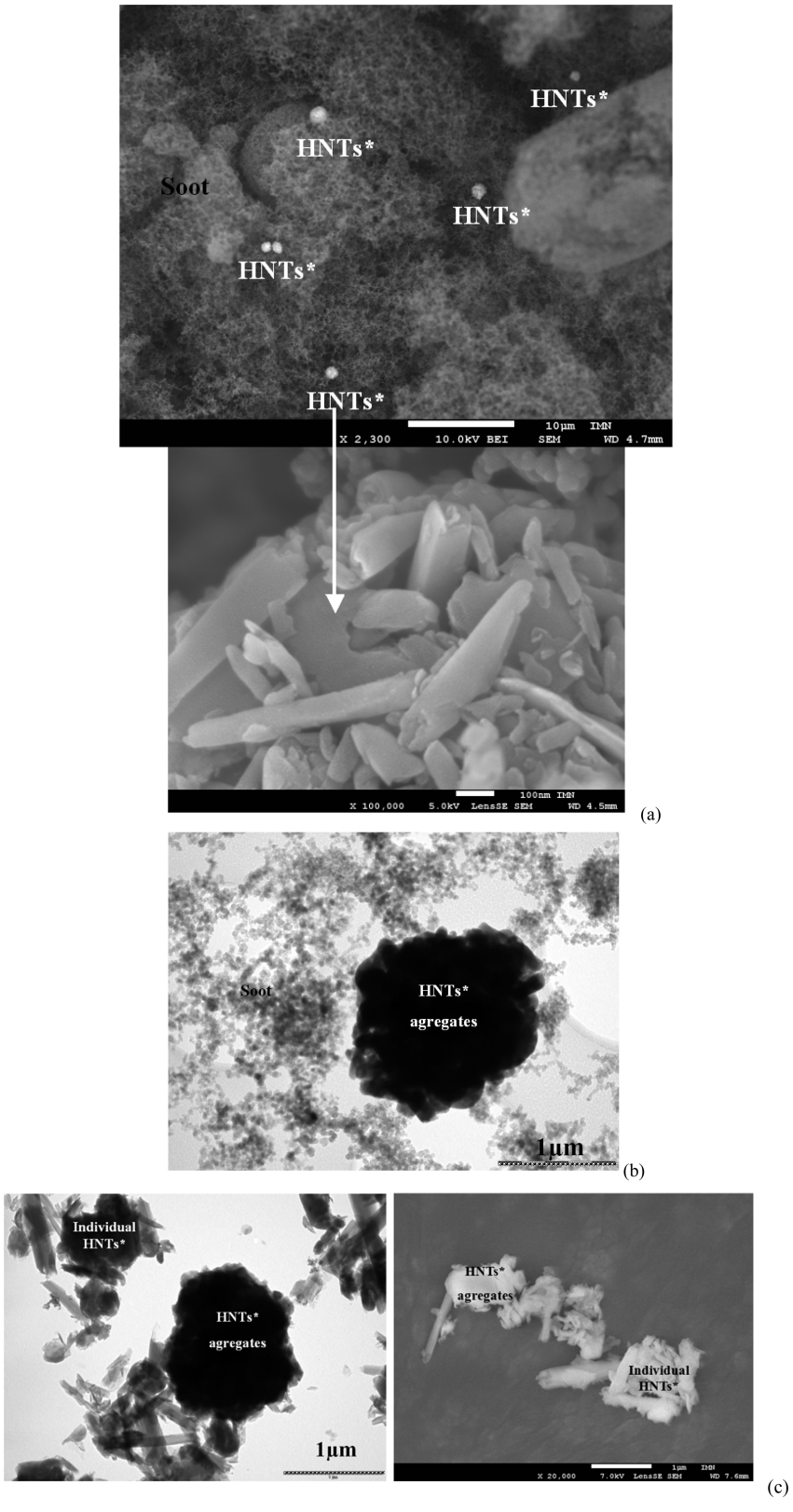

Figure 4. (a) Combustion aerosol particles collected on PTFE impaction substrate: soot and HNTs*, (b) Combustion aerosol particles collected on TEM grid: soot and HNTs* aggregates, (c) Combustion residues: HNTs* aggregates and individual HNTs*.

4.2. Imagery. The results from imagery provide only qualitative considerations.

HNTs* are defined as pseudo-HNTs with transformed mineral structures from HNTs.

4.2.1. Combustion Aerosol Particles. Imagery on particles collected on PTFE impaction substrates reveals the presence of HNTs* among the soot particles as shown in Figure 4a. These particles are from the fourth stage with dp50 = 1 μm. Submicron

HNTs* aggregates represent a minor fraction. Figure 4b shows the particles collected on a TEM grid during ten seconds preceding AOI. Submicron HNTs* aggregates are also minor components among the soot particles.

4.2.2. Combustion Residues. TEM and SEM (coupled with X-ray microanalysis) performed on combustion residues reveal that the residues are entirely inorganic and seem to consist of mineral aggregates and individual mineral particles (Figure 4c). No residues remain for the neat matrix case since neat PA6 decomposes completely.

4.2.3. TGA and PCFC on Nanocomposite. Figure 5 presents TGA curves of neat matrix, pristine HNTs and PA6/5HNTs.

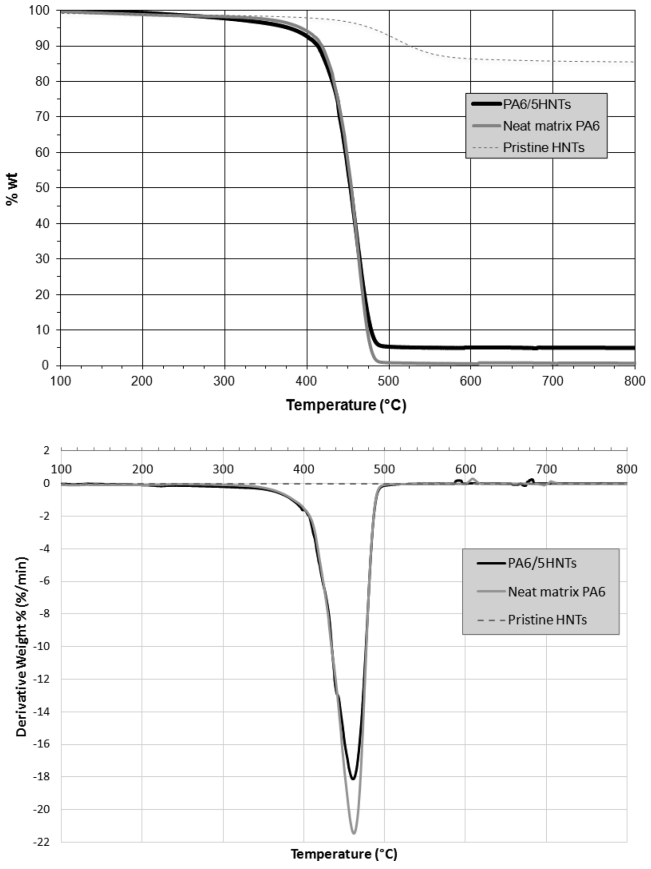

Figure 5. TGA under N_2.

The mass loss of HNTs (14%wt) corresponds to water release and occurs mainly in the 350−600 °C range. The mass loss range of PA6 occurs between 350 and 500 °C. It can be noticed that the presence of HNTs reduces the degradation onset temperature and the thermal stability up to 450 °C.

The incorporation of HNTs in PA6 reduces the PCFC peak (463 W/g for the pristine PA6 and 459 W/g for the composite). Besides, the shift toward high temperatures is almost unnoticeable because it is correlated with a mixing law (Figure 5). Nevertheless, PCFC peaks coincide roughly with the derivates of TGA curves (Figure 5, Figure 6). For both techniques, the thermal degradation of PA6 occurs at lower temperatures in the presence of HNTs.

4.2.4. XRD on Pristine HNTs and Residues. For pristine HNTs, X-ray fluorescence analysis (SI Table S3) and X-ray diffraction pattern (Figure 7) highlight that quartz (cristobalite) is present (nodular shape) as impurity of halloysite. The presence

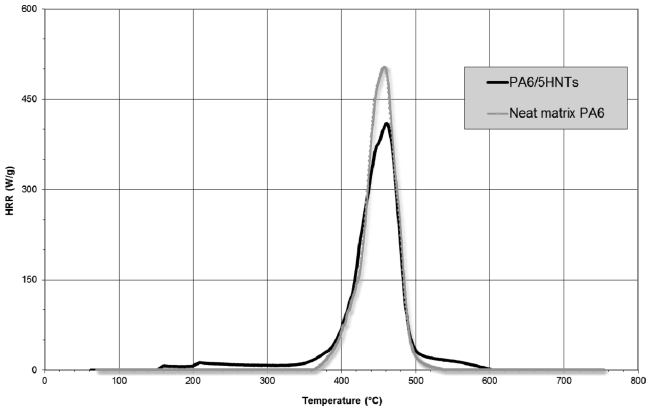

Figure 6. Heat Rate Release at PCFC of neat matrix and PA6/5HNTs nanocomposite.

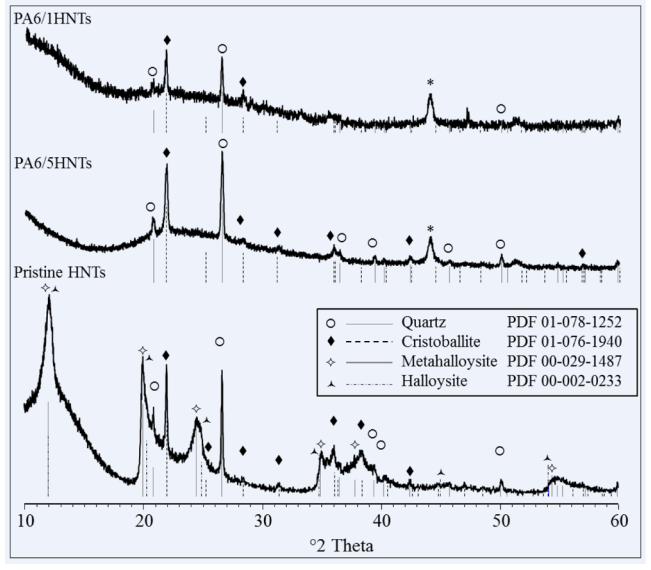

Figure 7. XRD of pristine HNTs and residues of nanocomposites.

of quartz leads to an excess of silicon over aluminum, since in pure halloysite, their ratio is 1:1.

XRD spectra performed on residues show that they essentially contain cristobalite and quartz. A bump can be noticed for the residue from PA6/5HNTs (between $2\theta = 20$ to 30°) which can be ascribed to an amorphous alumino-silicate structure. Only a peak at 44° was not identified. A temperature of at least 850 °C is attained in the furnace. Consequently, no halloysite remains in the residue even if SEM micrographs show pseudotubular structures, also for individual particles.

5. DISCUSSION

Considering the results about time tracking and imagery, interpretations can be proposed concerning the behavior and fate of HNTs during the incineration of PA6/HNTs nanocomposites.

5.1. HNTs Behavior: A Two Step Mechanism. First of all, a clear difference exists between the neat matrix and the nanocomposite. A two-step mechanism can be considered for PA6/HNTs nanocomposite. The evidence for this is the second CO peak, the NO_x shoulder, and the second phase in the emission of particles. Thus, the presence of HNTs is clearly responsible for this two step mechanism.

It takes around 15 s to introduce the sample in the furnace. This step involves particle emissions due to aerodynamic disturbance from the set up and due to the first thermal effects on the sample. Then, from 15 to 50 s, the thermal decomposition of the sample is indicated by the release of gases and particles, and by the presence of a flame for a few seconds. Effectively, as shown by TGA (Figure 5), HNTs lose water, so a hydrolysis of PA6 occurs and there is an increase in the release of volatile combustibles.[36] Furthermore, during this step, according to the literature, it is assumed that due to the thermal ablation of the polymer and the dehydration of HNTs, decohesion occurs between the PA6 and the HNTs.[25,37] Through these processes, the HNTs concentration at the surface of the sample increases and a protective layer gradually forms. TEM observation of particles collected during this phase reveals the presence of HNTs (in small quantities). The high concentration at the surface would promote the release of HNTs and make them free from the matrix and able to be carried away by the aerosol flow.

As reported in the literature, polyamide 6 could be considered as a charring polymer and the nanoclays as char promoters.[24,38] In fact, during a thermal decomposition, some materials can develop on their surface a protective layer which limits mass transfer (volatile combustible and oxygen transfer) as well as thermal transfer. Actually, CO time tracking with a double peak is a good indicator of the protective layer evolution. It was established that the decomposition of charring polymer involve two phases of gas release: the first one is associated with the primary char formation and the second one with the decomposition of the nonstable primary char.[39,40] Hence in the present case, the protective layer can be made of a carbonaceous char reinforced by HNTs. This char/HNTs layer forms progressively, since under-ventilated combustion occurs with a significant increase in CO emissions (Figure 3c). Simultaneously, the particle emission decreases from 45 s up to 70 s (Figure 3a) which is in agreement with the formation of a cohesive char layer. After 65s which corresponds to a CO peak, CO emission decreases and reaches a local minimum while oxygen consumption rises dramatically. This corresponds to the oxidation of the primary char.[39,40] Moreover, this oxidation is accompanied by an increase in particle emissions, which is irregular and suggests a partial cracking of the protective layer. So the second peak of $PN_{0.1}$ reflects the presence of a second combustion event. Furthermore, the NO_x shoulder from 100 s reflects the oxidation of the residual material which is no longer protected by the cracked char/HNTs layer (Figure 3d).

At the end of the combustion test, the residues from PA6/5HNTs incineration consist only of mineral compounds derived from the initial HNTs objects. However, some studies report carbon/clay residues after pyrolysis tests on polymer/clay nanocomposites[37] and especially for PA6/HNTs nanocomposites.[16] This difference should come from the combustion conditions implemented in the furnace. In fact, in our case the sample is well oxygenated at high temperature (850 °C or more) and for a high rate of increase in temperature (from 25 to 850 °C in 10 s). Therefore, under our incineration conditions, combustion is complete and no organic residues remain in the sample holder.

As with other nanoclays (montmorillonite for example), HNTs are known to have fire-retardant properties when incorporated in a polymer matrix.[16,17] During exposure to a heat source, these refractory materials can protect the matrix in which they are incorporated through the formation of a protective clay barrier which acts as a screen toward mass and heat transfers. The fire retardancy conferred by HNTs is confirmed by both the reduction in the peak heat release rate (pHRR) observed with the PCFC and the two-step mechanism discussed above. But this retardant character is not effective enough since it has been established that more than 15%wt is necessary to meet fire retardancy standards for industrial applications.[16]

The comparison between neat PA6 matrix and PA6/5HNTs nanocomposite shows that CO emission is stronger for the nanocomposite with a first peak at lower time. Besides, this tendency is confirmed for PA6/1HNTs (Figure 3c) with its CO curve just inserted between the two other CO curves. This suggests better char formation in the presence of HNTs. This easier char formation could be related to the lower thermal stability for the composite shown by TGA and PCFC, which indicate that the release of water from the clays leads to hydrolysis of PA6 polymer chains. Since the emission of particles is significantly lower for neat PA6, it shows that the char is more unstable with the unfilled polymer, and burns more easily.

We can thus surmise that the HNTs modify the thermal behavior of the PA6/HNTs nanocomposite during its incineration and that the more HNTs incorporated in PA6, the more the phenomenon is accentuated. In fact, these nanoclays enhance PA6's ability to form a protective char layer, and reinforce it via a cohesive char/HNTs layer. To sum up, through a two-step mechanism as suggested by analysis of the time tracking, this char/HNTs layer gradually forms, acts as a barrier, cracks, oxidizes and ends up entirely inorganic.

5.2. Fate of HNTs: Aggregates in Aerosol and Residues. The imagery results reveal the presence of mineral nano-objects in both the combustion aerosol and the combustion residues as aggregates and as prismatic (pseudotubular) structures which could result from partial distortion of the tubular structure.

Thus, HNTs are not destroyed during the incineration of PA6/HNTs nanocomposites, but seem to be transformed into other mineral structures (named HNTs*). Only qualitative considerations can be discussed here.

At high temperatures (beyond 1000 °C), the tubular morphology tends to distort and then halloysite transforms into new crystalline or amorphous structures such as gamma-alumina, cristobalite, and mullite.[41−43] Actually, it is established that thermal decomposition of HNTs occurs in three steps: dehydration (loss of H_2O from ∼200 °C), dehydroxylation (loss of OH from ∼500 to 900 °C) and a mullite-like phase formation (from 1200 to 1400 °C). The distortion of the tubular structure begins from 1000 °C and fusion up to 1400 °C.[41−43] Considering the high temperatures reached in the furnace (at least 850 °C and more in the presence of a flame), the HNTs undergo the aforementioned thermal transitions during the incineration of PA6/HNTs. Thus, the presence of mineral aggregates identified as pseudo-HNTs with transformed mineral structures (HNTs*) could be explained by the thermal process occurred during the HNTs' stay in the furnace, and the aggregated state could also be explained by a sintering process occurring during the stay above 850 °C. Nevertheless, the temperature is not high enough to ensure the crystallization of mullite.

Finally, regarding the behavior of multilayered silicates, it can be suggested that for the incineration of other PA6/silicate nanocomposites, mineral nano-objects could be found both in the aerosol downstream of the postcombustion chamber and in residues, but possibly transformed into other mineral structures, taking into account the temperature of the incinerator and the residence time. This should be confirmed by prospective additional incineration tests on other nanocomposites.

5.3. Concerns about Incineration of Waste Containing Nanomaterials.

A nanomaterial can be defined as any intentionally manufactured material, containing particles, in an unbound state or as an aggregate or as an agglomerate and where, for 50% or more of the particles in the number size distribution, one or more external dimensions is in the size range 1−100 nm, according to the European Commission article 18(5) of Regulation 1169/2011.[44] Their potential releases in the environment during their life cycle and their subsequent impacts on health have been an increasing concern for many years. Toxic effects of different types of nanomaterials have been studied and demonstrated.[45,46] Nevertheless, the data are incomplete and detailed studies are required.

The aim of the present study was to provide an insight into hazards regarding the incineration of waste containing nanomaterials from nanocomposites. Therefore, lab-scale tests were performed to investigate the release of nano-objects downstream of the postcombustion chamber and the presence of nano-objects in slag residues. Nano-objects from nanocomposites were found in the combustion aerosol and in residues. This leads to the conclusion that both flue gas and slag treatments would be affected by concerns about nanomaterial incineration and the potential precautions to be taken.

AUTHOR INFORMATION

Corresponding Authors

*(J.-M.L.-C.) E-mail: Jose-Marie.Lopez-Cuesta@mines-ales.fr.

*(O.L..B.) E-mail: Olivier.LE-BIHAN@ineris.fr.

Notes

The authors declare no competing financial interest.

ACKNOWLEDGMENTS

Financial support for this work was provided by ADEME, INERIS, and LNE. We are grateful to their colleagues from INERIS, Trédi (Séché Environnement), C2MA (Centre des matériaux des Mines d'Alès), IMN (Institut des Matériaux de Nantes) for their advice and technical support. Special thanks go to Anthony Chesnaud (Centre des Matériaux de Mines ParisTech) and Dr Gwenn Le Saout (Centre des Matériaux des Mines d'Alès) for their respective contributions to TEM imagery and X-ray diffraction.

REFERENCES

(1) Gao, F. Clay/polymer composites: The story. *Mater. Today.* **2004**, *7* (11), 1−72 DOI: 10.1016/S1369-7021(04)00509-7.

(2) Jang, B. N.; Wilkie, C. A. The effect of clay on the thermal degradation of polyamide 6 in polyamide 6/clay nanocomposites. *Polymer.* **2005**, *46* (10), 3264−3274 DOI: 10.1016/j.polymer.2005.02.078.

(3) Giannelis, E. P. Polymer-Layered Silicate Nanocomposites: Synthesis, properties and applications. *Appl. Organometal. Chem.* **1998**, *12*, 675−680 DOI: 10.1002/(SICI)10990739(199810/11)12:10/113.0.CO;2-V.

(4) Cho, J. W.; Paul, D. R. Nylon 6 nanocomposites by melt compounding. *Polymer.* **2001**, *42* (3), 1083−1094 DOI: 10.1016/S0032-3861(00)00380-3.

(5) Roes, L.; Patel, M. K.; Worrell, E.; Ludwig, C. Preliminary evaluation of risks related to waste incineration of polymer nanocomposites. *Sci. Total Environ.* **2012**, 417−418 76−86 DOI: 10.1016/j.scitotenv.2011.12.030.

(6) Walser, T.; Limbach, L.-K.; Brogioli, R.; Erismann, E.; Flamigni, L.; Günther, D.; Stark, W.-J. Persistence of engineered nanoparticles in a municipal solid-waste incineration plant. *Nat. Nanotechnol. Lett.* **2012**, *7*, 520−524 DOI: 10.1038/NNANO.2012.64.

(7) Mueller, N. C.; Buha, J.; Wang, J.; Ulrich, A.; Nowack, B. Modeling the flows of engineered nanomaterials during waste handling. *Environ. Sci.: Processes Impacts.* **2013**, *15*, 251−259 DOI: 10.1039/C2EM30761H.

(8) Holder, A. L.; Vejerano, E. P.; Zhou, X.; Marr, L. C. Nanomaterial disposal by incineration. *Environ. Sci. Process Impacts.* **2013**, *15*, 1652−1664 DOI: 10.1039/C3EM00224A.

(9) Vejerano, E. P.; Holder, A. L.; Marr, L. C. Emissions of Polycyclic Aromatic Hydrocarbons, Polychlorinated Dibenzo-p-Dioxins, and Dibenzofurans from Incineration of Nanomaterials. *Environ. Sci. Technol.* **2013**, *47*, 4866−4874 DOI: 10.1021/es304895z.

(10) Vejerano, E. P.; Leon, E. C.; Holdera, A. L.; Marr, L. C. Characterization of particle emissions and fate of nanomaterials during incineration. *Environ. Sci.: Nano* **2014**, *1*, 133−143 DOI: 10.1039/C3EN00080J.

(11) Massari, A.; Beggio, M.; Hreglich, S.; Marin, R.; Zuin, S. Behavior of TiO2 nanoparticles during incineration of solid paint waste: A lab-scale test. *Waste Management.* **2014**, DOI: 10.1016/j.wasman.2014.05.015.

(12) Stahlmecke, B.; Asbach, C.; Todea, A.; Kaminski, H.; Kuhlbusch, T. A. J. Investigations on CNT Release from Composite Materials During End of Life. In *Handbook of Nanosafety: Measurement, Exposure and Toxicology*; Elsevier, Eds.; Vogel, U., Savolainen, K, Wu, Q., van Tongeren, M., Brower, D., Berges, M. 2014; pp242−255.

(13) Fornes, T. D.; Paul, D. R. Modeling properties of nylon 6/clay nanocomposites using composite theories. *Polymer* **2003**, *44*, 4993−5013 DOI: 10.1016/S0032-3861(03)00471-3.

(14) Guo, B.; Zou, Q.; Lei, Y.; Jia, D. Structure and Performance of Polyamide 6/Halloysite Nanotubes Nanocomposites. *Polym. J.* **2009**, *41* (10), 835−842 DOI: 10.1295/polymj.PJ2009110.

(15) Hedicke-Höchstötter, K.; Lim, G. T.; Altstädt, V. Novel polyamide nanocomposites based on silicate nanotubes of the mineral halloysite. *Compos. Sci. Technol.* **2009**, *69*, 330−334 DOI: 10.1016/j.compscitech.2008.10.011.

(16) Marney, D. C. O.; Russell, L. J.; Wu, D. Y.; Nguyen, T.; Cramm, D.; Rigopoulos, N.; Wright, N.; Greaves, M. The suitability of halloysite nanotubes as a fire retardant for nylon 6. *Polym. Degrad. Stab.* **2008**, *93*, 1971−1978 DOI: 10.1016/j.polymdegradstab.2008.06.018.

(17) Liu, M.; Jia, D.; Zhou, C. Recent advance in research on halloysite nanotubes-polymer nanocomposite. *Prog. Polym. Sci.* **2014**, DOI: 10.1016/j.progpolymsci.2014.04.004.

(18) Du, M.; Guo, B.; Jia, D. Newly emerging applications of halloysite nanotubes: A review. *Polym. Int.* **2010**, *59*, 574−582 DOI: 10.1002/pi.2754.

(19) Kamble, R.; Ghag, M.; Gaikawad, S.; Panda, B. K. Halloysite nanotubes and applications: A review. *J. Adv. Scient. Res.* **2012**, *3*, 25−29 DOI: 10.1002/pi.2754.

(20) Bouillard, J.; R'mili, B.; Moranviller, D.; Vignes, A.; Le Bihan, O.; Ustache, A.; Bomfim, J. A.; Frejafon, E.; Fleury, D. Nanosafety by design: Risks from nanocomposite/nanowaste combustion. *J. Nanopart. Res.* **2013**, *15*, 15−19 DOI: 10.1007/s11051-013-1519-3.

(21) Motzkus, C.; Chivas-Joly, C.; Guillaume, E.; Ducourtieux, S.; Saragoza, L.; Lesenechal, D.; Macé, T.; Lopez-Cuesta, J.-M.; Longuet, C. Aerosols emitted by the combustion of polymers containing nanoparticles. *J. Nanopart. Res.* **2012**, *14*, 1−17 DOI: 10.1051/rfm/2012009.

(22) Chivas-Joly, C.; Motzkus, C.; Guillaume, E.; Ducourtieux, S.; Saragoza, L.; Lesenechal, D.; Lopez-Cuesta, J.-M.; Longuet, C.; Sonnier, R.; Minisini, B. Influence of carbon nanotubes on fire behaviour and aerosol emitted during combustion of thermoplastics. *Fire Mater.* **2014**, *38*, 46−62 DOI: 10.1002/fam.2161.

(23) Rhodes, J.; Smith, C.; Stec, A. Characterisation of soot particulates from fire retarded and nanocomposite materials, and their toxicological

impact. *Polym. Degrad. Stab.* **2011**, *96*, 277−284 DOI: 10.1016/j.polymdegradstab.2010.07.002.
(24) Kashiwagi, T.; Harris, R. H.; Zhang, X.; Briber, R. M.; Cipriano, B. H.; Raghavan, S. R.; Awad, W. H.; Shields, J. R. Flame retardant mechanism of polyamide 6−clay nanocomposite. *Polymer* **2004**, *45*, 881−891.
(25) Lewin, M.; Pearce, E. M.; Levon, K.; Mey-Marom, A.; Zammarano, M. C. A.; Wilkie Jang, B. N. Nanocomposites at elevated temperatures: Migration and structural changes. *Polym. Adv. Technol.* **2006**, *17*, 226−234 DOI: 10.1002/pat.684.
(26) Walters, R. N.; Lyon, R. E. Molar group contributions to polymer flammability. *J. Appl. Polym. Sci.* **2003**, *87*, 548−563 DOI: 10.1002/app.11466.
(27) BREF Waste Incineration 2006, Reference document on best available techniques http://www.ineris.fr/ippc/sites/default/files/files/wi_bref_0806.pdf (accessed on June 2014).
(28) Niemelä V., Lamminen E., Laitinen A. A Novel method for particle sampling and size-classified electrical charge measurement at power plant environment. In *11th International Conference on Electrostatic Precipitation*, 2009.
(29) Andersson J., Mamakos A., Giechaskiel B., Carriero M., Martini G. *Particle Measurement Programme (PMP) Heavy-Duty Inter-Laboratory Correlation Exercise (ILCE_HD) Final Report*, GRPE-PMP-25-05. 2010.
(30) Motzkus, C.; Chivas-Joly, C.; Guillaume, E.; Ducourtieux, S.; Saragoza, L.; Lesenechal, D.; Mace, T.; Lopez-Cuesta, J.-M.; Longuet, C. Aerosols emitted by the combustion of polymers containing nanoparticles. *J. Nanopart. Res.* **2012**, *14*, 1−17 DOI: 10.1007/s11051-011-0687-2.
(31) Tissari, J.; Hytonen, K.; Lyyranen, J.; Jokiniemi, J. A novel field measurement method for determining fine particle and gas emissions from residential wood combustion. *Atmos. Environ.* **2007**, *41*, 8330−8344 DOI: 10.1016/j.atmosenv.2007.06.018.
(32) Keskinen, J.; Pietarinen, K.; Lehtimaki, M. Electrical low pressure impactor. *J. Aerosol Sci.* **1992**, *23*, 353−360 DOI: 10.1016/0021-8502(92)90004-F.
(33) Lyyränen, J.; Jokiniemi, J.; Kauppinen, E. I.; Backman, U.; Vesala, H. Comparison of different dilution methods for measuring diesel particle emissions. *Aerosol Sci. Technol.* **2004**, *38*, 12−23 DOI: 10.1080/02786820490247579.
(34) Sarvi, A.; Lyyränen, J.; Jokiniemi, J.; Zevenhoven, R. Particulate emissions from large-scale medium-speed diesel engines: 2. Chemical composition. *Fuel Process. Technol.* **2011**, *92*, 2116−2122 http://dx.doi.org/10.1016/j.fuproc.2011.06.021.
(35) R'mili, B.; Le Bihan, O.; Dutouquet, C.; Aguerre-Chariol, O.; Frejafon, E. Particle sampling by TEM grid filtration. *Aerosol Sci. Technol.* **2013**, *47* (7), 767−775 DOI: 10.1080/02786826.2013.789478.
(36) Davis, R. D.; Gilman, J. W.; Vander Hart, D. L. Processing degradation of polyamide 6/montmorillonite clay nanocomposites and clay organic modifier. *Polym. Degrad. Stab.* **2003**, *79*, 111−121 DOI: 10.1016/S0141-3910(02)00263-X.
(37) Vaia, R. A.; Price, G.; Ruth, P. N.; Nguyen, H. T.; Lichtenhan, J. Polymer layered silicate nanocomposites as high performance ablative materials. *Appl. Clay Sci.* **1999**, *15*, 67−92 DOI: 10.1016/S0169-1317(99)00013-7.
(38) Gilman, J. W.; Kashiwagi, T.; Harris, R. H. Jr.; Lomakin, S. M.; Lichtenhan, J. D.; Bolf, A.; Jones, P. Char enhancing approaches to flame retarding polymers, *Chem. Technol. Polym. Addit.*. 1999, Chapter 8, Blackwell Science Inc., Malden, MA, Ak-Malaika, S.; Golovoy, A.; Wilkie, C. A., 135−150.
(39) Bahramian, A. R.; Kokabi, M.; Famili, M. H. N.; Beheshty, M. H. High temperature ablation of kaolinite layered silicate/phenolic resin/asbestos cloth nanocomposite. *J. Hazard. Mater.* **2008**, *150*, 136−145 DOI: 10.1016/j.jhazmat.2007.04.104.
(40) Lyon, R. E. Pyrolysis kinetics of char forming polymers. *Polym. Degrad. Stab.* **1998**, *61*, 201−210 DOI: 10.1016/S0141-3910(97)00125-0.
(41) Yuan, P.; Tan, D.; Annabi-Bergaya, F.; Yan, W.; Fan, M.; Liu, D.; He, H. Changes in structure, morphology, porosity, and surface activity of mesoporous halloysite nanotubes under heating. *Clays Clay Miner.* **2012**, *60*, 561−573 DOI: 10.1346/CCMN.2012.0600602.
(42) Cheng, H.; Frost, R.; Yang, J.; Liu, Q.; He, J. Infrared and infrared emission spectroscopic study of typical Chinese kaolinite and halloysite. *Spectrochim. Acta* **2010**, *77* (Part A), 1014−1020 DOI: 10.1016/j.saa.2010.08.039.
(43) Smith, M. E.; Neal, G.; Trigg, B. M.; Drennan, J. Structural characterization of the thermal transformation of halloysite by solid state NMR. *Appl. Magn. Reson.* **1993**, *4*, 157−170 DOI: 10.1007/BF03162561.
(44) Potocnick J. European Commission Recommendation on the definition of nanomaterial, 2011/696/EU, 2011.
(45) Wang, Q.; Yang, Z.; Yanga, Y.; Long, C.; Li, H. A bibliometric analysis of research on the risk of engineering nanomaterials during 1999−2012*Sci. Total Environ.* **2014**, 473−474, 483−489; DOI: http://dx.doi.org/10.1016/j.scitotenv.2013.12.066.
(46) Kühnel, D.; Nickel, C. The OECD expert meeting on ecotoxicology and environmental fate—Towards the development of improved OECD guidelines for the testing of nanomaterials. *Sci. Total Environ.* **2014**, *472*, 347−353 http://dx.doi.org/10.1016/j.scitotenv.2013.11.055.